

The Mid-infrared View of Red Sequence Galaxies in Abell 2218 with *AKARI*

Jongwan Ko^{1,2}, Myungshin Im^{1,2}, Hyung Mok Lee¹, Myung Gyoon Lee¹, Ros H. Hopwood³, Stephen Serjeant³, Ian Smail⁴, Ho Seong Hwang⁵, Narae Hwang⁶, Hyunjin Shim¹, Seong Jin Kim¹, Jong Chul Lee¹, Sungsoon Lim¹, Hyunjong Seo¹, Tomotsugu Goto⁷, Hitoshi Hanami⁸, Hideo Matsuhara⁹, Toshinobu Takagi⁹, and Takehiko Wada⁹

jwko@astro.snu.ac.kr

ABSTRACT

We present the *AKARI* InfraRed Camera (IRC) imaging observation of early-type galaxies in A2218 at $z \simeq 0.175$. Mid-infrared (MIR) emission from early-type galaxies traces circumstellar dust emission from AGB stars or/and residual star formation. Including the unique imaging capability at 11 and 15 μm , our *AKARI* data provide an effective way to investigate MIR properties of early-type galaxies in the cluster environment. Among our flux-limited sample of 22 red sequence early-type galaxies with precise dynamical and line strength measurements (< 18 mag at 3 μm), we find that at least 41% have MIR-excess emission. The $N3 - S11$ versus $N3$ (3 and 11 μm) color-magnitude relation shows the expected blue sequence, but the MIR-excess galaxies add a red wing to the relation especially at the fainter end. A SED analysis reveals that the dust emission from AGB stars is the most likely cause for the MIR-excess, with low level of star formation being the next possible explanation. The MIR-excess galaxies show a wide spread of $N3 - S11$ colors, implying a significant spread (2–11 Gyr) in the estimated mean ages of stellar populations. We study the environmental dependence of MIR-excess early-type galaxies over an area out to a half virial radius (~ 1 Mpc). We find that the MIR-excess early-type galaxies are preferentially located in the

¹Astronomy Program, Department of Physics & Astronomy, FPRD, Seoul National University, Seoul 151-742, Korea

²Center of the Exploration of the Origin of the Universe (CEOEU), Seoul National University, Seoul, Korea

³Department of Physics and Astronomy, Open University, Walton Hall, Milton Keynes MK7 6AA, UK

⁴Institute for Computational Cosmology, Department of Physics, Durham University, South Road, Durham, DH1 3LE, UK

⁵Korea Institute for Advanced Study, Seoul 130-722, Korea

⁶National Astronomical Observatory of Japan, Mitaka, Tokyo 181-8588, Japan

⁷Institute for Astronomy, University of Hawaii 2680 Woodlawn Drive, Honolulu, HI, 96822, USA

⁸Physics Section, Faculty of Humanities and Social Sciences, Iwate University, Morioka 020-8550, Japan

⁹Institute of Space and Astronautical Science, Japan Aerospace Exploration Agency, Kanagawa 229-8510, Japan

outer region. From these evidences, we suggest that the fainter, MIR-excess early-type galaxies have just joined the red sequence, possibly due to the infall and subsequent morphological/spectral transformation induced by the cluster environment.

Subject headings: galaxies: clusters: individual: Abell 2218 — galaxies: elliptical and lenticular — galaxies: stellar content — infrared: galaxies

1. INTRODUCTION

Early-type galaxies (ETGs hereafter) are the dominant population in galaxy clusters. Their stellar population is thought to be homogeneously old and passively evolving as shown in the tight color-magnitude (CM) relation (e.g., Bower et al. 1992; Kodama & Arimoto 1997).

This picture of ETGs consisting of homogeneous stellar population breaks down when we examine their properties at different wavelengths. It is known from earlier infrared observations that some ETGs exhibit excess far-infrared emission (Knapp et al. 1989), and mid-infrared emission (Knapp et al. 1992; Xilouris et al. 2004). The observation in UV also confirms a diversity of ETGs (Smail et al. 1998; Yi et al. 2005; Schawinski et al. 2007). A particular interest can be placed on the mid-infrared (MIR) emission. Recently, Clemens et al. (2008) found that about 32% of ETGs in the Coma cluster have excess flux over photospheric emission at MIR.

This MIR-excess can be due to various mechanisms, such as emission from circumstellar dust around AGB stars (Knapp et al. 1992), star formation, and AGN activities (Quillen et al. 1999). Recent Spitzer observations indicate that the origin of the MIR-excess is the dusty AGB stars for the majority of ETGs in the red sequence (Bressan et al. 2006). According to the model where the MIR-excess is caused by the dust emission from AGB stars, the MIR-excess is prominent if the luminosity weighted mean age of the stellar populations is young (Piovan et al. 2003, hereafter P03).

ETGs with MIR-excess could be used as a tracer of morphological transformation in the cluster environment. For example, star-forming spiral galaxies infalling to a cluster have been suspected that they would be morphologically transformed into quiescent S0s through various physical processes (e.g., Dressler et al. 1997; Goto et al. 2003; Boselli & Gavazzi 2006; Park & Hwang 2008) leaving relatively young ETGs showing MIR-excess. However, such an analysis has limited due to the paucity of complete MIR ($7 - 24 \mu\text{m}$) imaging observation covering a large field around a cluster of galaxies.

In this paper, we examine the relation between the cluster environment and the MIR-excess of ETGs in A2218, a galaxy cluster at $z = 0.175$ (e.g., Biviano et al. 2004), using *AKARI* space telescope (Murakami et al. 2007) that offers a wide-field imaging of the galaxy cluster at 11 and 15 μm for the first time. A2218 is a rich cluster (richness class = 4) with a virial radius of $(1.5 - 2.3)$ Mpc and a mass of $(4.8 - 21) \times 10^{14} M_{\odot}$ (Girardi & Mezzetti 2001; Pratt et al. 2005).

A2218 has been observed by the Infrared Space Observatory (ISO), and the previous ISO study revealed the lack of MIR-excess early-type galaxies at the central region of A2218 (Biviano et al. 2004), while the analysis of optical/NIR imaging and spectroscopy of this cluster have shown a wide dispersion in the stellar ages of faint ETGs (Smail et al. 2001; Ziegler et al. 2001; Sanchez et al. 2007). The two results seem contradictory, and a wide-field IR imaging could offer a solution.

Throughout this paper, we use $H_0 = 70 \text{ km s}^{-1}\text{Mpc}^{-1}$, $\Omega_m = 0.3$ and $\Omega_\Lambda = 0.7$ (Spergel et al. 2003). In this cosmology, the angular scale of 1 arcsec at the distance of this galaxy cluster corresponds to 2.97 kpc. All magnitudes are given in the AB system.

2. THE DATA AND THE SAMPLE

2.1. Data

The rich cluster A2218 is one of the targets selected for studying low redshift clusters by the *CLusters of galaxies EVoLution studies* (CLEVL, PI: H. M. Lee; Im et al. 2008), an *AKARI* mission program aiming to understand the formation and evolution of galaxies in cluster environments. The *AKARI* observation for the A2218 field was carried out using 6 broadband filters¹ (*NIR*: *N3*, *N4*, and *MIR*: *S7*, *S11*, *L15*, *L24*) of the InfraRed Camera (IRC; Onaka et al. 2007) onboard the *AKARI*. We covered a $15 \times 15 \text{ arcmin}^2$ field centered on the X-ray brightness peak of A2218, using 4 IRC tiles. The image depth differs according to the locations, and the central $5 \times 5 \text{ arcmin}^2$ region is the deepest. Table 1 lists the total exposure time and the 5σ point-source detection limit over $11''$ diameter aperture in this region. The flux limit at the outer region is $\sqrt{2}$ or 2 times shallower than the central region.

The raw images were processed and stacked with the IRC imaging data reduction pipeline version 070104 and then co-added into one final mosaic image using SWarp². Cosmic rays were rejected during the stacking. Additional removal of cosmic rays was carried out using L.A.Cosmic (van Dokkum 2001) when necessary. We checked if this procedure causes flux loss using the North Ecliptic Pole Survey data of *AKARI* (Matsuhara et al. 2006; Wada et al. 2008; Lee et al. 2009), and found no significant flux loss.

We used SExtractor (Bertin & Arnouts 1996) to detect sources. The measured ADUs were converted to the Jy unit using the conversion factors from the IRC manual version 1.4. When doing the flux calibration for extended sources, we additionally considered color correction since the IRC flux calibration assumed $f_\lambda \propto \lambda^{-1}$. We calculated the correction factor following the method provided in the IRC manual with the model SEDs of P03. We find that the color correction can affect the flux value at $\lesssim 10\%$ level, but $\sim 22\%$ flux change occurs in extreme cases. Since it is

¹Numbers next to each alphabet indicate central wavelengths

²http://terapix.iap.fr/rubrique.php?id_rubrique=49.

difficult to know the SED shape a priori, we leave the color correction as unknown systematic error.

We used the MAG-AUTO to estimate the total magnitude. To check the MAG-AUTO as the total magnitude for all band, we estimated large aperture photometry of several isolated galaxies in the final image, and found that the difference between MAG-AUTO and MAG-APER was within typical measurement errors (NIR: $\lesssim 3\%$, MIR: $\lesssim 20\%$). However, especially in the NIR band, FLUX-AUTO of sources with close neighbors are affected by nearby sources. To derive fluxes of such objects, we used small circular aperture of $5.''5$ diameter and applied aperture corrections that are derived from the growth curve of isolated galaxies with similar flux.

For the central $10' \times 10'$ region, we also used a deeper L15 image taken for another *AKARI* program (PI: Serjeant) to derive $15 \mu\text{m}$ fluxes. The 5σ detection limit of the deep L15 image is 20.1 mag, and the details on this data will be presented elsewhere (Hopwood et al. in preparation).

Additionally, we used optical fluxes (*UBVI*) from Ziegler et al. (2001, hereafter Z01), and $24/70 \mu\text{m}$ data taken by the *Spitzer*/MIPS (GTO program #83, PI: G. Rieke) in the archive for the overlapping region with *AKARI* where the MIPS $24 \mu\text{m}$ image is deeper than the *AKARI* image.

2.2. Sample

For the sample selection, we started with 48 ETGs of A2218 of the central $9.7 \times 9.7 \text{ arcmin}^2$ in Z01 and additional cluster members whose redshifts were obtained from the NASA/IPAC Extragalactic Database (NED) search of the central $15 \times 15 \text{ arcmin}^2$ area of A2218 ($z=0.165 - 0.185$). The morphology of 9 sources added from the NED search is determined to be ETGs by the visual inspection of the archival optical images (CFHT and Subaru) and SED shapes. These galaxies were matched with the *AKARI* source catalog, and we checked each member whether it is blended or not in the *AKARI* image by comparing with the optical images. Through this process, we excluded galaxies that are blended with neighbors in the *AKARI* image. Finally, we collected 39 (30 from Z01) non-blended ETGs from the *AKARI* data. Among these we have selected a sample of 22 galaxies with $N3 < 18 \text{ mag}$ for MIR-excess study.

3. RESULTS & DISCUSSION

3.1. The color-magnitude relation

In Figure 1, we show the CM diagram of A2218 galaxies in three colors; $U - V$ (a), $N3 - N4$ (b), and $N3 - S11$ (c). The $N3$ flux is chosen to be on the x-axis, as a rough measure of the stellar mass (e.g. Gavazzi et al. 1996). The $U - V$ versus $N3$ CM diagram is shown for galaxies with $N3 < 18 \text{ mag}$. It shows a usual tight red sequence of ETGs, with two galaxies (#665 and #2139

in Z01) slightly bluer than the others. This reflects the fact that Z01 sample is made of galaxies belonging to the red sequence or close to it. Figure 1b shows the $N3 - N4$ versus $N3$ CM relation. The plot shows a tight blue sequence since the flux decreases as the wavelength increases at $\lambda > 1.6 \mu\text{m}$. Next, we have examined the MIR ($S11$) properties of galaxies selected using a box shown in Figure 1b, i.e., galaxies with $N3 < 18$ mag. This magnitude cut is imposed due to the relatively shallower $S11$ detection limit, so that we can construct an unbiased sample in $N3 - S11$ colors.

Figure 1c shows the $N3 - S11$ versus $N3$ CM relation of the cluster members with $N3 < 18$ mag. Also plotted are the CM relations from various model SEDs (see below). At the bright end, four galaxies tend to form a blue sequence indicating that they are a homogeneous population. However, Figure 1c reveals a stunningly wide dispersion in the $N3 - S11$ colors of the optical red sequence galaxies with $N3 > 17$ mag. More than $\sim 50\%$ show MIR-excess at $N3 > 17$ mag above the model line considering photospheric emission only (the “old noAGB” line). This is in clear contrast to the result of Biviano et al. (2004) where a small fraction of ETGs showed this kind of MIR-excess.

To understand what is causing the MIR-excess, we compared the observed CM relation with the model predictions. For the model SEDs, we used Single Stellar Population (SSP) models with a spontaneous burst, the Salpeter (1955) IMF, and the Padova Library of stellar spectra from P03 which also incorporates the dust emission from circumstellar dust around AGB stars. As it has been recognized, the optical CM relation can be described well with a single age model assuming a metallicity gradient (the dashed line in Fig. 1a; e.g., Kodama et al. 1997). The same model fits the $N3 - S11$ versus $N3$ CM relation at the bright magnitude (the solid line in Fig. 1c), but it fails to reproduce the dispersion in the $N3 - S11$ colors of the fainter ETGs. The dispersion requires the existence of stellar populations with younger ages, or some other mechanisms.

In the top panel of Figure 2, we examine the MIR-excess of ETGs in more detail by plotting $N3 - S11$ versus $N3 - N4$ color-color diagram. The thick solid line indicates the track of a SSP as described in the dashed line of Figure 1a but with several different ages (1~15 Gyrs). The other lines indicate the tracks of model SEDs with the AGB circumstellar dust of P03. We define MIR-excess galaxies to be those lying at the redward of the dotted line. This corresponds to the MIR-excess more than typical 1σ error of ($N3 - S11$) color (~ 0.28 mag) over the thick solid line. Among galaxies in our magnitude limited sample, more than 41% (9/22) can be classified as galaxies having MIR-excess. In the lower panels of Figure 2, MIR-excess galaxies have relatively low velocity dispersion. Although considering our flux-limited sample, this result suggests that less massive ETGs are more likely to have MIR-excess than massive ones. However, MIR-excess does not show strong correlation with $H\beta$ line index which is sensitive to recent star formation activity. It is very possible that $H\beta$ line and MIR-excess trace different epoch in star formation history, but it seems difficult to draw a firm conclusion on this based on the current data alone.

Figure 3 shows the observed optical-MIR SEDs of nine $S11$ -detected galaxies. We performed the least square fit of SEDs using three different models – spectral synthesis models with or without

AGB dust from P03 (*AGB* or *noAGB* model), and templates of star-forming galaxies from Chary & Elbaz (2001). The best-fit SEDs from each model are overplotted in Figure 3. The SSP models of P03 have three different metallicities ($Z = 0.02, 0.008, 0.004$) and a wide range of ages (0.1~15 Gyrs). In case of the fit to the SF model, we do not use the optical data for the fit, since the empirical SF SED templates do not include the diverse optical SEDs with different ages, metallicities, and star formation histories.

Based on the significance of MIR-excess, we categorize the sample into three sub-groups; strong-, mid-, and weak/no MIR-excess galaxies. First, we note that the P03 *noAGB* model fails to fit the strong/mid MIR-excess galaxies, but provides reasonable fits to the weak/no ones.

Next, we find that most ETGs with MIR-excess returned acceptable SED fits to the P03 *AGB* model with either a solar or 40% solar metallicities. The lowest metallicity P03 model (20% solar) can fit the MIR-excess if we consider the IR portion of the SEDs alone, but such a model fails to fit the optical portion of the SEDs. The results suggest that the MIR-excess correlates with ages more strongly than metallicities, with a distinct trend that the younger galaxies have the stronger MIR-excess (Temi et al. 2005). For the MIR-excess ETGs, the derived mean stellar ages span a wide range of 2 to 11 Gyr, which qualitatively agrees with the findings by Smail et al. (2001) and Biviano et al. (2004). This suggests that the MIR-excess is a good indicator of mean stellar ages of ETGs, as also noted by Temi et al. (2005).

The AGB dust emission is not the only possible cause for the MIR-excess. We caution that the MIR-excess may arise from the star-forming activities and AGNs. In some cases, it is difficult to exclude such possibilities from the current data alone. Deeper 70 μm data could offer an effective way to test these possibilities. However, even if the MIR-excess arises from the star-forming activity, the derived SFRs from the SED fits suggest $\text{SFR} < 1M_{\odot} \text{ yr}^{-1}$ for all of the MIR-excess galaxies. The only exception is #697 in Z01 which shows an abnormally high 15 μm flux. It is difficult to explain such a flux with the P03 *AGB* model. This may be a piece of evidence for existence of PAH emissions from star formation for this galaxy. The morphology of this galaxy seems to show a disk. The objects #1914, and #2139 have spiky 11 μm fluxes, which may be due to unusual PAH features at 11.3 and 12.7 μm found in some ETGs (e.g. Kaneda et al. 2005).

We conclude that more than half of cluster ETGs with $N3 < 18$ mag are likely to have the MIR-excess over stellar photospheric emission, which we interpret as the emission from circumstellar dust around AGB stars. Our result is different from the ISOCAM study of Biviano et al. (2004) where they did not find such MIR-excess for most of ETGs in A2218. This can be attributed partly to the deeper depth of our data, but mostly to our much wider area coverage.

3.2. Environmental dependence of MIR-excess

To investigate the MIR properties of A2218 ETGs as a function of the cluster environment, we plot the spatial and velocity distributions of 39 *AKARI* cluster ETGs with the contour maps of

the *Chandra* X-ray emission in Figure 4. MIR-excess ETGs seem not to have a preference for the velocity distribution, but the clustercentric-distance distribution of them is exceptional.

We expect to find younger, MIR-excess galaxies in the outskirts of the cluster if such galaxies are formed via transformation from field spirals accreted to the cluster environment. To check this, we divide our samples into those closer to the center and those in the outer region depending on the cluster-centric distance (at 381 kpc) in the same manner of Z01.

We find that about 64% (7/11) of the outer galaxies have MIR-excess, while only 18% (2/11) of the inner ones do so. These MIR-excess galaxies are also relatively faint ones in our sample. We remark that there are ETGs in the inner region as faint as the MIR-excess ETGs in the outer region, but they do not show clear MIR-excess. From these results, we conclude that these MIR-excess galaxies are fainter, and preferentially located in the outer region of the cluster, suggesting that they could be the descendants of the infalling field galaxies transformed into ETGs. Our conclusion appear to be reconciled with the result of Z01 where they found larger spread of $H\beta$ values of A2218 cluster ETGs in the outskirts. We are carrying out similar studies using 6 more nearby clusters to obtain a more conclusive answer.

We thank L. Piovan for providing his SED model. We also thank the referee, Bodo Ziegler, for his constructive comments which improved our paper. This work is based on observations with *AKARI*, a JAXA project with the participation of ESA. We acknowledge the Creative Research Initiatives program, CEOU of MEST/KOSEF. RHH, SBGS, and IRS also acknowledge support from STFC.

REFERENCES

- Bertin, E. & Arnouts, S. 1996, *A&AS*, 117, 393
- Biviano, A. et al. 2004, *A&A*, 425, 33
- Boselli, A., & Gavazzi, G. 2006, *PASP*, 118, 517
- Bower, R. G., Lucey, J. R. & Ellis, R. S. 1992, *MNRAS*, 254, 601
- Bressan, A. et al. 2006, *ApJ*, 639, L55
- Chary, R. & Elbaz, D. 2001, *ApJ*, 556, 562
- Clemens, M. S. et al. 2008, *MNRAS*, in press (astro-ph/0808.2899)
- Dressler, A. et al. 1997, *ApJ*, 490, 577
- Gavazzi, G., Pierini, D. & Boselli, A. 1996, *A&A*, 312, 397

- Girardi, M. & Mezzetti, M. 2001, *ApJ*, 548, 79
- Goto, T. et al. 2003, *MNRAS*, 346, 601
- Im, M. et al. 2008, *ASPC*, 399, 382
- Knapp, G. R. et al. 1989, *ApJS*, 70, 329
- Knapp, G. R., Gunn, J. E. & Wynn-Williams, C. G. 1992, *ApJ*, 399, 76
- Kodama, T. & Arimoto, N. 1997, *A&A*, 320, 41
- Kaneda, H., Onaka, T. & Sakon, I. 2005, *ApJ*, 632, L83
- Lee, H. M. et al. 2009, *PASJ*, in press
- Matsuhara, H. et al. 2006, *PASJ*, 58, 673
- Maughan, B. J. et al. 2008, *ApJ*, 174, 117
- Murakami, H. et al. 2007, *PASJ*, 59, S369
- Onaka, T. et al. 2007, *PASJ*, 59, S401
- Park, C., & Hwang, H. S. 2008, *ApJ*, submitted (astro-ph/0812.2088)
- Piovan, L., Tantalò, R. & Chiosi, C. 2003, *A&A*, 408, 559
- Pratt, G. W., Böhringer, H. & Finoguenov, A. 2005, *A&A*, 433, 777
- Quillen, A. C. et al. 1999, *ApJ*, 518, 632
- Salpeter, E. E. 1995, *ApJ*, 121, 161
- Sanchez, S. F. et al. 2007, *MNRAS*, 376, 125
- Schawinski, K. et al. 2007, *ApJS*, 173, 512
- Spergel, D. N. et al. 2003, *ApJS*, 148, 175
- Smail, I. et al. 2001, *MNRAS*, 323, 839
- Smail, I. et al. 1998, *MNRAS*, 293, 124
- Temi, P., Mathews, W. G. & Brighenti, F. 2005, *ApJ*, 622, 235
- van Dokkum, P. G. 2001, *PASP*, 113, 1420
- Wada, T. et al. 2008, *PASJ*, 60, S517
- Xilouris, E. M. et al. 2004, *A&A*, 416, 41

Yi, S. K. et al. 2005, ApJ, 619, L111

Ziegler, B. L. et al. 2001, MNRAS, 325, 1571

Table 1. Observational parameters of the A2218 data

Filter name	Effective wavelength [μm]	Total Integration time [second]	5σ point-source sensitivity (within $11''$ ap.) [AB mag.]
N3	3.2	710.6	21.3
N4	4.1	710.6	21.5
S7	7.2	392.7	20.0
S11	10.4	490.9	19.6
L15	15.9	785.4	19.3
L24	23.0	785.4	18.3

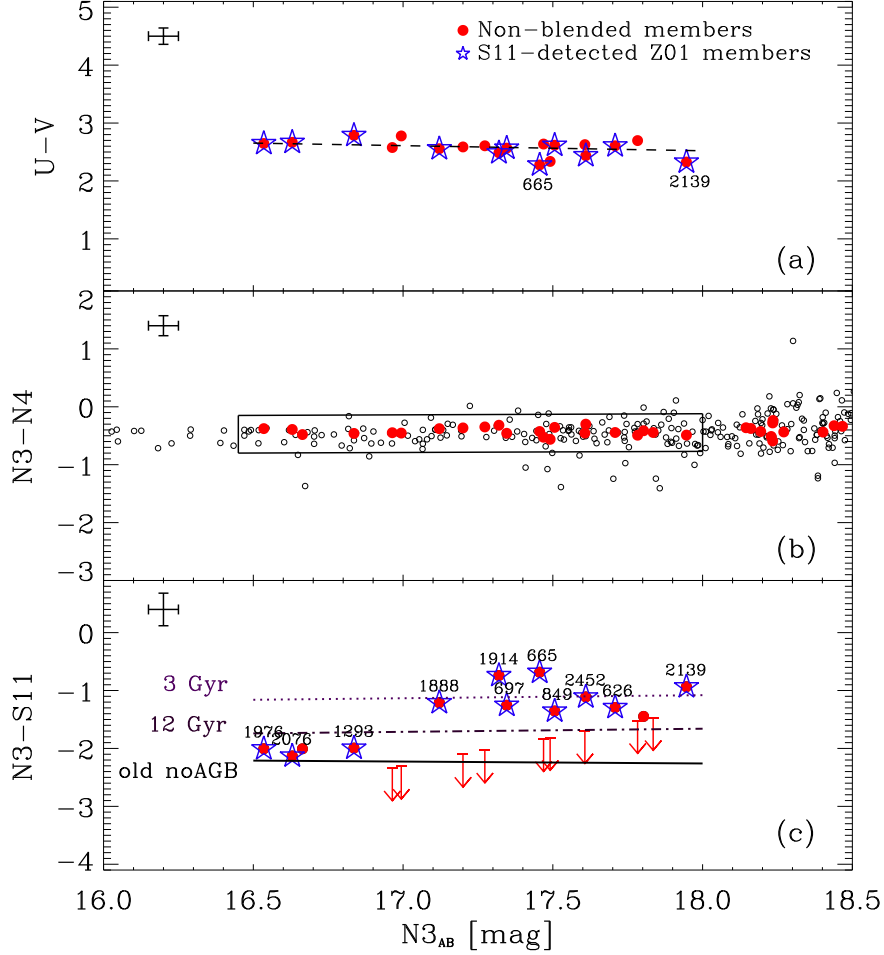


Fig. 1.— *Top*: The $U - V$ vs. $N3$ CM diagram for $N3$ flux limited ETGs. Filled circles indicate our non-blended ETGs, and among them Z01 members detected in $S11$ are represented by star symbols. The galaxy numbers (#665 and #2139) are the notation used by Z01. The dashed line represents the best-fit $U - V$ vs. $N3$ CM relation. The cross in the upper left corner indicates the median errors. *Middle*: The $N3 - N4$ vs. $N3$ CM diagram of *AKARI* IRC imaging sample. Open circles are all sources detected in the 15×15 arcmin² field. Due to the detection limit of the $S11$ flux, we select bright ($N3 < 18$) sources. *Bottom*: The $N3 - S11$ vs. $N3$ CM diagram for the galaxies in the box of panel (b). The 3σ detection limit are given for sources undetected in $S11$ (arrows). The dotted and the dashed-dotted lines indicate the CM relation calculated from the P03 *AGB* model SEDs assuming the metallicity gradient at two different stellar ages (3 and 12 Gyr), respectively. The solid line represents the 12 Gyr P03 *noAGB* model, assuming the metallicity sequence that fits the $U - V$ vs. $N3$ CM relation.

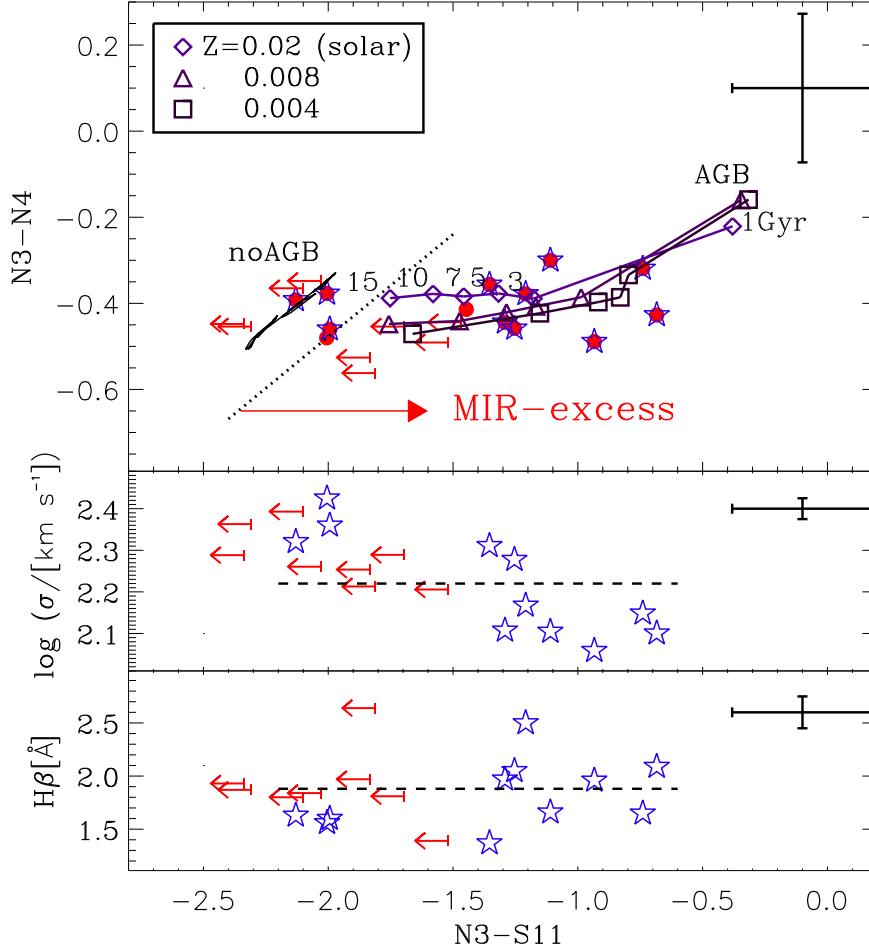


Fig. 2.— *Top*: The $N3 - N4$ vs. $N3 - S11$ color-color diagram for galaxies in the box of Fig. 1b. Symbols have the same meanings as Fig. 1c. The diamond, triangle, and square symbols represent loci of the P03 *AGB* models along mean stellar ages (1, 3, 5, 7, 10, and 15 Gyr) for $Z=0.02$ (solar metallicity), 0.008, and 0.004, respectively. The thick solid line shows the P03 *noAGB* model color. *MIR-excess* galaxies as those redder than dotted line in $N3-S11$ (1σ redder than the P03 *noAGB* model). The cross represents the median errors. *Middle*: The velocity dispersion vs. $N3 - S11$ color for Z01 data available. Symbols as the upper panel. The dashed line represents the mean value of σ for 48 ETGs in Z01. *Bottom*: $H\beta$ line index vs. $N3 - S11$ color for Z01 data available. Symbols as the upper panel. The dashed line represents the mean value of $H\beta$ line indices for 48 ETGs in Z01.

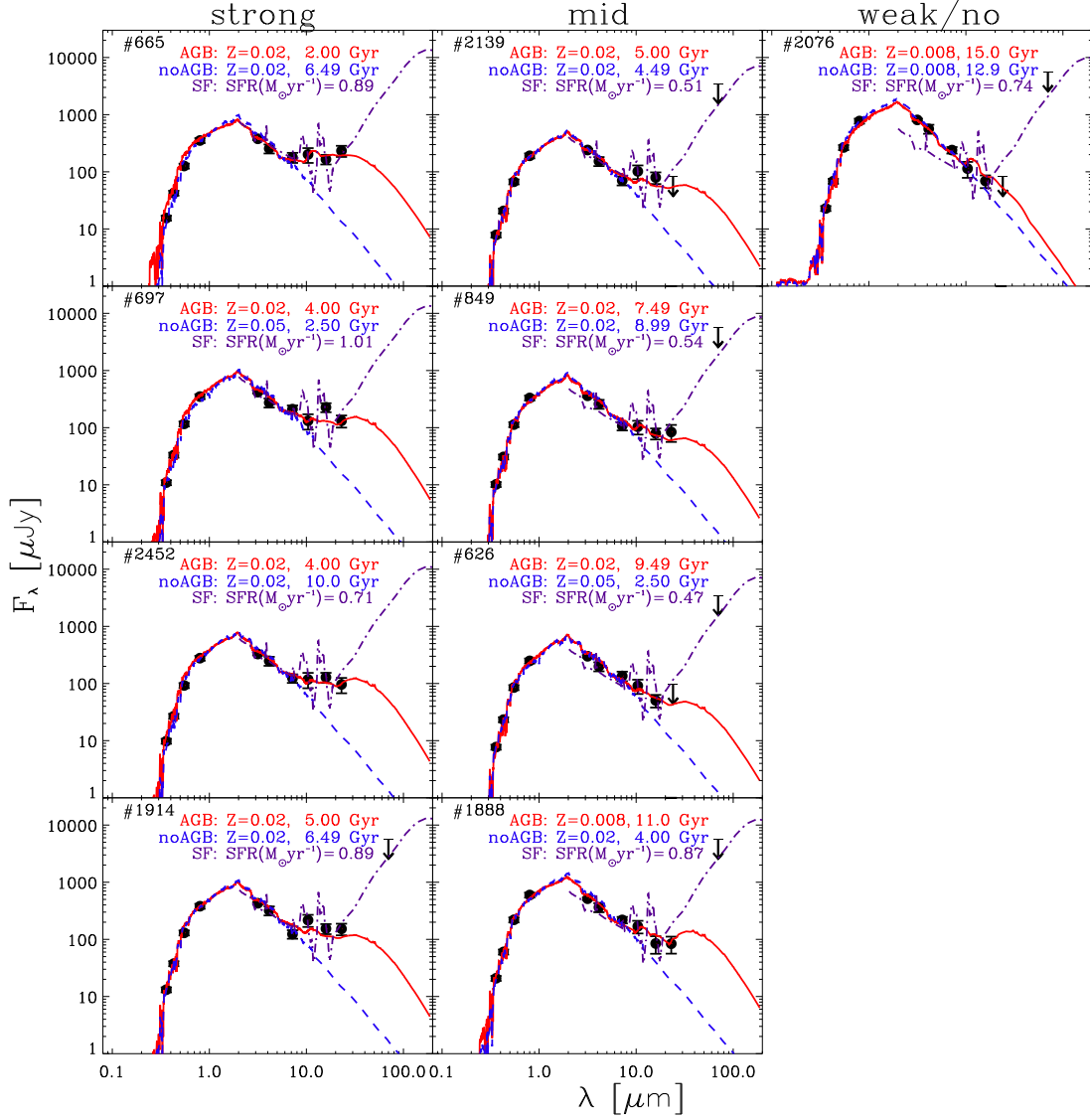


Fig. 3.— The observed SEDs of the S11-detected galaxies with Z01 optical and the *Spitzer* 24/70 μm data available. The best-fit lines of three different models (AGB: solid, noAGB: dashed, SF: dashed-dotted) are overplotted with 1σ error bars. Arrows represent the 3σ detection limit.

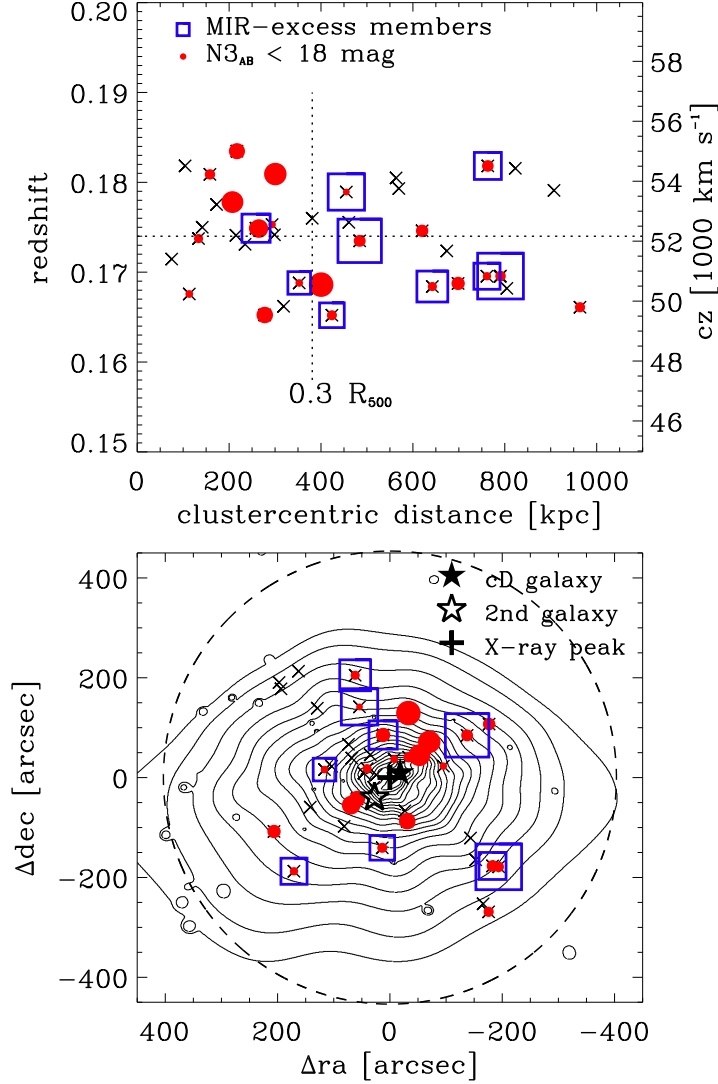


Fig. 4.— *Upper*: The clustercentric distance and velocity distributions for the 39 A2218 *AKARI* cluster ETGs (‘x’ symbols). Filled circles are ETGs with $N3 < 18$ mag, and the size is proportional to $N3$ flux. The squares are MIR-excess galaxies as defined in Fig. 2, and the size is proportional to F_{11}/F_3 flux density ratios (mass-normalized MIR-excess). The vertical dotted line indicates the radius to divide into two bins and R_{500} is usually known as roughly half of the virial radius (1.21 Mpc from Maughan et al. 2008). *Lower*: The spatial distribution overlaid with the adaptively-smoothed X-ray contours adopted from Maughan et al. Symbols as the upper panel. The cross, the filled star, and the open star indicate the position of the X-ray brightness peak, the cD galaxy, and the 2nd brightest cluster galaxy, respectively. The dashed circle corresponds to the radius R_{500} .